

Rings in Fireball Afterglows

A. Panaitescu & P. Mészáros

Pennsylvania State University, 525 Davey Lab., University Park, PA 16802

ABSTRACT

We derive the equation for the surface of equal arrival time of radiation from a thin relativistic shell interacting with an external medium, representing the afterglow of a gamma-ray burst produced by a fireball. Due to the deceleration, these surfaces become distorted ellipsoids and, at sufficiently late times, most of the light (either bolometric or in a given band) comes from a ring-like region whose width depends only on age. We analyze the shape of these surfaces and the radiation received from different angles for different dynamic and radiative regimes and homogeneous or power-law external densities. We calculate angle-integrated bolometric and fixed frequency fluxes, and we tabulate the most relevant parameters that describe the equal arrival time surfaces and the source brightness distribution, quantities that are useful for more accurate analytic estimates of the afterglow evolution.

Subject headings: gamma-rays: bursts - methods: analytical

1. Introduction

The afterglows of gamma-ray bursts (GRB) appear to be well-fitted by decelerating relativistic fireball models (Tavani, 1997; Vietri, 1997; Waxman, 1997a; Wijers, Rees & Mészáros, 1997). This picture (Mészáros & Rees, 1997), in its simplest form, assumes that the bulk of the radiation comes from the external blast wave pushed ahead of the fireball with a diminishing bulk Lorentz factor, which is predicted to produce radiation at wavelengths longer than γ -rays decaying as a power-law in time, in good agreement with observations. Two interesting consequences of the deceleration dynamics are that most of the late radiation comes from a narrow ring, rather than the entire visible surface (Waxman, 1997b), and that the usual estimate for the transverse size of a relativistically expanding cloud under-estimates the real one (as we show in §3). This has consequences for the apparent expansion rate of the fireball, the evolution of scintillation properties of the radio-emitting remnant (Goodman, 1997; Frail et al, 1997), and the probability of microlensing of GRB afterglows (Loeb & Perna, 1997). The exact shape of the surface, the dimensions and the expansion rate depend on the dynamic and radiative regimes, as well as on assumed properties of the external medium. We present detailed analytical and numerical

calculations of these properties taking into account the effects of the dynamic and radiative efficiency regimes, for both homogeneous and power-law density external media. We investigate the equal arrival time surfaces and source apparent width evolution, provide estimates of the width of the rings, and present simple analytic expressions for both the “average” longitudinal and transverse sizes, in the cases of either bolometric or fixed frequency band observations.

2. Equal Arrival Time Surfaces

Here we derive the equation of the surface that the observer sees at given time T . For simplicity, we assume that the source of radiation can be approximated as a surface (see §4 for a discussion on this approximation). We also assume the external medium to be isotropic, but not necessarily homogeneous; therefore at any lab-frame time t (measured in the center of explosion frame), the ejecta is spherical. The observer equal- T surface is symmetric with respect to the line of sight (l.o.s.) toward the center of explosion which released the relativistic ejecta, therefore its equation is given by two coordinates: a polar angle θ measured from this central l.o.s. and a radial coordinate r . In the absence of deceleration, the equal- T surface is an ellipsoid (Rees 1966) with semi-major axis $\Gamma^2\beta cT$ and semi-minor axis $\Gamma\beta cT$, where $\Gamma = (1 - \beta^2)^{-1/2}$ is the constant Lorentz factor of the freely expanding ejecta and c is the speed of light. For large Γ , the ellipsoid is very elongated (high eccentricity). When deceleration is present, the shape of the equal- T surface departs from that of an ellipsoid.

The equation of the equal detector time T surface is

$$ct - r(t) \cos \theta = cT, \quad (1)$$

where r and t are related by $dr = \beta_{sh} c dt$, with $\beta_{sh} c$ the speed of the shock that sweeps up the external medium. The Lorentz factor γ_{sh} of this shock can be approximated (e.g. Mészáros, Rees & Wijers, 1997) as a power-law in r :

$$\gamma_{sh} = \Gamma_{sh} (r/r_{dec})^{-n} \quad ; \quad n = \frac{3 - \alpha}{1 + \delta} > 0, \quad (2)$$

where α (< 3) is the index of external gas density power law dependence ($\rho \propto r^{-\alpha}$), δ describes the dynamics ($\delta = 0$ for momentum-conserving and $\delta = 1$ for energy-conserving evolution), and r_{dec} is the deceleration radius, defined as the radius at which the ejecta has swept up a mass equal to a fraction Γ_0^{-1} of its own mass, Γ_0 being the initial Lorentz factor of the ejecta. Numerical simulations of the hydrodynamic interaction between the ejecta and the external medium (Panaitescu & Mészáros, 1997) show that γ_{sh} slowly decreases below the deceleration radius r_{dec} and that $\Gamma_{sh} \simeq (2/3)\Gamma_0$. Thus equation (2) is correct only for $r > r_{dec}$.

For relativistic shocks, the relationship between t and r has a simple form:

$$ct = r + \frac{r_{dec}}{2(2n + 1)\Gamma_{sh}^2} \left(\frac{r}{r_{dec}} \right)^{2n+1}. \quad (3)$$

Substituting t from equation (3) in equation (1), the equal- T surface is

$$\theta = 2 \sin^{-1} \left(\frac{1}{2\Gamma_{sh}} \sqrt{\frac{\tau}{a} - \frac{a^{2n}}{2n+1}} \right), \quad (4)$$

where the reduced variables $a = r/r_{dec}$ and $\tau = T/T_{dec}$ with $T_{dec} \equiv r_{dec}/(2\Gamma_{sh}^2 c)$ have been used. T_{dec} is the time-scale for the onset of the deceleration given in equation (2). At given T , the fluid moving directly towards the observer ($\theta = 0$) is located at

$$x_{max} = [(2n+1)\tau]^{1/(2n+1)} r_{dec}, \quad (5)$$

this being where the radius is largest and Lorentz factor is smallest on the surface, $\gamma_{sh,o} = [(2n+1)\tau]^{-n/(2n+1)} \Gamma_{sh}$. The relativistic shock condition $\gamma_{sh} \geq 2$ used in deriving equation (3) limits the applicability of equation (4) to $\tau \leq (2n+1)^{-1}(\Gamma_{sh}/2)^{2+1/n}$. As an example, we show in Figure 1 the equal- T surfaces at different values of τ , for $\Gamma_0 = 500$ (corresponding to $\Gamma_{sh} = 330$), for a homogeneous external medium ($\alpha = 0$). The times indicated in the legend correspond to 3.6 hours, 1.5 days, 5.0 days (and 15 days, right panel), if T_{dec} is taken as 13 seconds, which would be the value in a burst arising from $\Gamma_0 = 500$, an initial energy release of $E_0 = 10^{52}$ ergs/sr, and a redshift $z = 1$. (A jet of angle θ_{jet} reduces the energy required by a factor θ_{jet}^{-2} without changing the results, as long as $\gamma_{sh} \gtrsim \theta_{jet}^{-1}$).

It is customary in analytic derivations to consider that at a given time T the emitting surface is located at $r = 2\gamma^2(T)cT$, and that the disk seen by the observer has a radius $R = r/(2\gamma(T)) = \gamma(T)cT$, as it would be in the absence of the deceleration (i.e. an ellipsoid), and to calculate the properties of the received radiation using the physical parameters (magnetic field, electron and flow Lorentz factor etc.) of the fluid located at $(x = r, y = 0)$, the center of the projected surface. When deceleration is present, the radial coordinate x_{max} of the center of the equal- T surface can be related to T by integrating $dT = dr/(2\gamma_{sh}^2 c)$ and using equation (2):

$$x_{max} = 4(2n+1)\gamma_o^2 cT, \quad (6)$$

where we used the flow Lorentz factor $\gamma_o \equiv \gamma(x_{max})$ instead of that of the shock $\gamma_{sh,o} = \sqrt{2}\gamma_o$. Therefore x_{max} is larger by a factor $2(2n+1)$ than the value that is typically used, $2\gamma_o^2 cT$. For $n = 1.5$ (adiabatic remnant and homogeneous external gas) one obtains in equation (6) a factor 16 (Sari 1997), but this factor could be as large as 28 for a strong coupling radiative remnant ($n = 3$). This differs substantially from the usual factor 2 in the longitudinal size. To estimate the corresponding departures in the largest transverse size y_{max} observable assuming the geometry of an ellipsoid for the equal- T surface in a decelerating fireball, we consider the projection of this surface on the plane perpendicular to the central l.o.s.

$$y_{max}^{ell} = x_{max}/(2\gamma_o) = 2(2n+1)\gamma_o cT. \quad (7)$$

The numerical factor in equation (7) is 8 for $n = 1.5$. Waxman (1997b) argued that such a large transverse size is incompatible with observations and that the correct transverse source

size is smaller by a factor 4 than that inferred using a factor 16 in equation (6). The large factor in equation (7) is due to the inappropriate use of the geometry of an ellipsoid in the case of a decelerated expansion. Since the transverse source size is important for self-absorption considerations, for the evolution of the timescale and amplitude of afterglow radio scintillations and for gravitational microlensing, it is worth calculating accurately the coefficient in equation (7) that gives the source size.

3. Characteristic Radiation and Dimensions

In order to determine the properties of the radiation received by the observer, one has to integrate over the surface of equal arrival time the emission from different parts of the shocked fluid, taking into account relativistic effects and the fact that each infinitesimal ring $[\theta, \theta + d\theta]$ is characterized by different physical parameters (magnetic field, electron density, electron Lorentz factor, flow Lorentz factor). We assume that the electrons cool only through synchrotron radiation (our numerical simulations show that this is a good approximation), and that they are either in the radiative or in the adiabatic regime. In the former case we take into account that the remnant can be either radiative or adiabatic, depending on the strength of the coupling between the radiating electrons, protons and the magnetic field (for more details on the radiative regime and the dynamics, see Mészáros, Rees & Wijers, 1997), while in the latter case the remnant can be only adiabatic (energy conservation). Using the scaling relationships for the magnetic field $B' \propto \gamma r^{-\alpha/2}$, the co-moving electron density $n'_e \propto \gamma r^{-\alpha}$, synchrotron cooling time-scale $t'_{sy} \propto r \gamma^{-3}$, expansion time-scale $t'_{exp} \propto \gamma^{-1} r$, synchrotron power $P'_{sy} \propto \gamma^4 r^{-\alpha}$ and peak of synchrotron spectrum $\nu'_p \propto \gamma^3 r^{-\alpha/2}$, where γ is the flow Lorentz factor, the co-moving spectral intensity at the synchrotron peak $I'_{\nu'_p} \propto n'_e (P'_{sy}/\nu'_p) \min \{t'_{sy}, t'_{exp}\}$ is

$$I'_{\nu'_p} \propto \begin{cases} \gamma^{-1} r^{-\alpha/2} & \text{for radiative electrons} \\ \gamma r^{1-3\alpha/2} & \text{for adiabatic electrons} \end{cases} \quad (8)$$

The observed spectral intensity at the detector frame peak of the synchrotron spectrum $\nu_p = \nu'_p / [\gamma (1 - \beta \cos \theta)]$ is $I_{\nu_p} = (\nu_p / \nu'_p)^3 I'_{\nu'_p}$, therefore

$$I_{\nu_p} \propto \begin{cases} a^{-(2n+\alpha/2)} (1 + \gamma^2 \theta^2)^{-3} & t'_{sy} < t'_{exp} \\ a^{-(4n+1.5\alpha-1)} (1 + \gamma^2 \theta^2)^{-3} & t'_{sy} > t'_{exp} \end{cases} \quad (9)$$

The bolometric co-moving intensity is $I' \sim I'_{\nu'_p}$, and the observed bolometric intensity is $I \sim (\nu_p / \nu'_p)^4 I'$. The synchrotron spectrum is approximated as a broken power-law: $I_\nu = (\nu / \nu_p)^\epsilon I_{\nu_p}$ below the peak ($\nu < \nu_p$) and $I_\nu = (\nu / \nu_p)^{-\varepsilon} I_{\nu_p}$ above the peak ($\nu > \nu_p$). We considered that $\epsilon = -1/2$ and $\varepsilon = p/2$ for radiative electrons and $\epsilon = 1/3$ and $\varepsilon = (p-1)/2$ for adiabatic electrons, p being the index of the power-law distribution of electrons (we used $p = 2.5$). The detector flux density is obtained by integrating I_ν over the equal arrival time surface, taking into account the solid angle subtended by each infinitesimal ring $[\theta, \theta + d\theta]$ on this surface.

We study first the bolometric brightness distribution on the equal- T surface. Figure 1 shows where most of the radiation comes from: the upper half highlighted zone radiates 50% of the total energy; 25% of it is emitted by the cap extending from $\theta = 0$ up to the indicated region and the other 25% is radiated by the area extending toward the origin. Similarly, the lower half highlighted part radiates 80% of the energy received at detector. Projecting any of these zones on the plane perpendicular to the central l.o.s. results in rings that are thin compared to the disk of the entire projected surface seen by the observer.

Apart from the errors mentioned at the end of §2, a new source of inaccuracy in analytic calculations of the source size and the radiation received comes from the fact that the observer does not receive most of the flux from the central l.o.s. of the deformed ellipsoid. There is a significant difference between the average radial coordinates of the regions highlighted in Figure 1 and that of the fluid on the l.o.s. toward the center, and one must keep in mind that all relevant radiation parameters are power-laws in γ , which is a power-law in r . We can assess the error in equation (7), obtained using the “ellipsoid approximation”, by calculating an intensity-weighted average transverse coordinate \bar{y} on the equal- T surface and comparing it to $\gamma_o cT$. We also calculate an intensity-weighted average longitudinal \bar{x} coordinate on the same surface and compare it with x_{max} from equation (6), so that the factor $(x_{max}/\bar{x})^n$ will estimate the difference between an average $\bar{\gamma}$ that should in general be used instead of γ_o . These averages are given in Table 1, which also lists the width w of the outer ring of the source projection on the plane perpendicular to the central l.o.s., which contains 50% of the entire flux received at detector. Also in Table 1 are the ratios between the intensity-averaged synchrotron peak frequency $\bar{\nu}_p$ over the T -surface, and $\nu_o \equiv \nu_p(\theta = 0)$. We find that the coefficient $2(2n + 1)$ in equation (7) over-estimates the true value of the transverse size \bar{y} by a factor $2.1 - 2.7$.

We consider now observations in a fixed frequency band. Figure 2 (upper graphs) shows the transverse distribution of the observed synchrotron peak frequency ν_p for various constant- T surfaces. The unknown coefficient in the expression for ν_p was chosen so that at $T \sim 1$ day (with $T_{dec} = 13$ s), most of the energy the observer receives is in the optical range (~ 2 eV). The lower graphs show the peak (or bolometric) luminosity integrated up to the transverse coordinate y as a function of y . The ring is indicated by the steep rise in the integrated luminosity, during which ν_p varies by approximately one order of magnitude around the peak frequency $\nu_p(y_{max})$ of the radiation from the region that is seen tangentially by the observer. If observations are made at energies $\lesssim 10^{-1} \nu_p(y_{max})$ (e.g. in radio, for the times chosen in Figure 2) then the observer practically sees only the low-energy part of slope $-1/2$ (or $1/3$) of the synchrotron spectrum of the radiation emitted from most points on the equal- T surface, and the entire disk appears almost equally bright. However, if observations are made at energies $\gtrsim 10 \nu_p(y_{max})$ (optical or X-ray for Figure 2), then the observer sees mainly the high-energy tail of slope $-(p - 1)/2$ (or $-p/2$) of the synchrotron spectrum from the power-law distribution of electrons, and the visible region reduces to a ring. For a given observed frequency band, as the shocked fluid is decelerated, $\nu_p(y_{max})$ crosses the observed band, and the region radiating in that band shrinks from the full

disk to a narrow ring with outer boundary at y_{max} , the edge of the radiating surface. During this transition \bar{x}/x_{max} decreases while \bar{y}/y_{max} increases. At energies far above or below $\nu_p(y_{max})$, these quantities and the width of the “visible” zone are approximately constant in time. Table 2 gives the asymptotic range of the same coefficients as Table 1, for observations made at a given frequency. The first number in each column gives the value of the coefficient when the source is seen as disk ($\nu \ll \bar{\nu}_p \sim \nu_p(y_{max})$, larger width w), and the last number gives the asymptotic value of the coefficient when the source has reduced to a ring ($\nu \gg \nu_p(y_{max})$, smaller w). The coefficients have the same range for all frequencies. The particular frequency of the observing band only determines the time when the gradual transition between the two coefficients is made, earlier in X-rays (few hours) than in optical (~ 1 day) or radio (~ 10 days). It can be seen that the radiative remnant gives narrower rings, and that the ring is wider for expansion into a decreasing density medium (e.g. $\alpha = 2$) than into a homogeneous medium ($\alpha = 0$).

4. Discussion

The main conclusions to be drawn from the calculations presented here are:

1. For the afterglow of a fireball, the equal arrival time surfaces are distorted ellipsoids whose shape and evolution depend on the dynamical regime of the remnant, the electron radiative efficiency and the density distribution of the external medium.
2. Equation (6) should be used to relate the observer time T with the radial coordinate of the center of this surface, and the size of the source should be calculated with an equation similar to (7) but with the coefficient $2(2n + 1)$ replaced by the coefficients in Table 1 for bolometric observations. For band observations these coefficients change in time; Table 2 gives only their upper and lower limits. This is of relevance for the scintillation of the afterglow in radio (Goodman, 1997; Frail et al, 1997).
3. The spectrum and intensity should be calculated using the gas parameters characteristic of the ring (rather than those of the l.o.s. to the center). The mean ratio between average peak frequency in the ring and in the central l.o.s. is given in Table 1. For a given dynamic and radiative regime this ratio is constant in time, thus the power-law time dependences of the observable flux predicted by the fireball afterglow models (Mészáros & Rees, 1997; Mészáros, Rees & Wijers, 1997) remain unchanged.
4. When observations are restricted to a narrow energy band, the shape (ring or disk) of the source seen by the observer is dependent on the observational band. In any band, the observer should see the source increasing in overall size and changing its shape from a full disk to a relatively narrow ring, at least while the expansion is relativistic. This is of importance for the possible gravitational microlensing of afterglows (Loeb & Perna 1997). If bolometric observations are obtained by piecing together band observations spanning many orders of magnitude, then most of the energy of the afterglow should be seen coming from a relatively narrow ring, at any time.

The thickness of the zone that radiates most of the energy is important because it determines

the spread δT in the arrival time of photons emitted at lab-frame t . Generally, δT is comparable to T . In the radiative case electrons cool on a time-scale much shorter than the expansion time, only a very thin zone located behind the blast wave front releases significant energy and the thickness of the radiating fluid can be neglected. Therefore in this case the emitting fluid can be safely approximated as a surface. The effect of the shell thickness is important only in the adiabatic case, and was taken in consideration by Waxman (1997b). We have employed here the equal arrival time surfaces using the kinematics of the blast wave. Radiation emitted by the fluid behind this shock is received at time $T > T_{sh}$, where T_{sh} is the arrival time from the blast wave. Taking into account that the source size is increasing in time, it results that a finite thickness leads to wider rings and lower values of the averages \bar{x} and \bar{y} given in Tables 1 and 2. Our estimations of the ring's width for an adiabatic remnant are larger by a factor up to 2.3 than calculated by Waxman (1997b).

Additional complications arise if different regions on the equal- T surface are in different dynamic and/or radiative efficiency regimes. As the fireball decelerates, the cooling time-scale of electrons increases and they eventually become adiabatic. If there is a strong coupling between electrons and protons + magnetic field, the remnant and electrons evolve together from the radiative to the adiabatic regime. In the likely case that the coupling is weak (e.g. Mészáros , Rees, & Wijers, 1997), the remnant evolution is adiabatic throughout, and only the electrons evolve from radiative to adiabatic. At times $\gtrsim 1$ day, the most likely case is given by the third (or sixth) line of Tables 1 and 2. The real situation may be even more complex if the power-law electrons are in different radiative regimes, e.g. low energy electrons may be adiabatic ($t'_{sy} > t'_{exp}$) while higher energy electrons may be radiative ($t'_{sy} < t'_{exp}$).

This research has been supported by NASA NAG5-2857 and NAG5-2362

REFERENCES

- Frail D., et.al., 1997, Nature, in press
- Goodman, J. 1997, New Astr., submitted (astro-ph/9706084)
- Loeb, A. & Perna, R. 1997, ApJL, submitted (astro-ph/9708159)
- Mészáros , P. & Rees, M. J. 1997, ApJ, 476, 232
- Mészáros , P., Rees, M. J. & Wijers, R., 1997, ApJ, submitted (astro-ph/9709273)
- Panaitescu, A. & Mészáros , P., 1997, ApJ, 492, in press (astro-ph/9703187)
- Rees, M. J. 1966, Nature, 211, 468
- Sari, R. 1997, astro-ph/9706078

Tavani, M., 1997, ApJL, 483, L87

Vietri, M., 1997, ApJ, submitted (astro-ph/9706060)

Waxman, E., 1997a, ApJL, 485, L5

Waxman, E. 1997b, ApJL, submitted (astro-ph/9709190)

Wijers, R.A.M.J., Rees, M.J. & Mészáros, P., 1997, MNRAS, 288, L51

TABLE 1.
INTENSITY-AVERAGED PARAMETERS ON THE EQUAL ARRIVING TIME SURFACE
AND THE WIDTH w OF THE RING SEEN BY THE OBSERVER FOR BOLOMETRIC OBSERVATIONS

$n [\alpha, \delta]$	$2(2n+1)$	\bar{x}/x_{max}	$\bar{x}/(2\gamma_o^2 cT)$	\bar{y}/y_{max}	$\bar{y}/(\gamma_o cT)$	$\bar{\nu}_p/\nu_o$	w
3.0 $[0, 0]^r$	14	0.78	11	0.87	5.2	39	0.07
1.5 $[0, 1]^r$	8	0.82	6.6	0.76	3.2	4.0	0.17
1.5 $[0, 1]^a$	8	0.72	5.8	0.82	3.4	8.3	0.11
1.0 $[2, 0]^r$	6	0.74	4.4	0.77	2.6	6.7	0.16
0.5 $[2, 1]^r$	4	0.78	3.1	0.71	1.8	2.0	0.23
0.5 $[2, 1]^a$	4	0.49	2.0	0.76	1.9	6.8	0.20

^r radiative electrons ^a adiabatic electrons

TABLE 2.
INTERVALS FOR INTENSITY-AVERAGED PARAMETERS ON THE EQUAL ARRIVING TIME SURFACE
AND WIDTH w OF THE RING SEEN BY THE OBSERVER FOR BAND OBSERVATIONS

$n [\alpha, \delta]$	\bar{x}/x_{max}	$\bar{x}/(2\gamma_o^2 cT)$	\bar{y}/y_{max}	$\bar{y}/(\gamma_o cT)$	w
3.0 $[0, 0]^r$	0.88–0.72	12–10	0.77–0.89	4.6–5.4	0.16–0.06
1.5 $[0, 1]^r$	0.87–0.78	7.0–6.3	0.70–0.79	2.9–3.3	0.25–0.13
1.5 $[0, 1]^a$	0.89–0.77	7.1–6.2	0.67–0.79	2.8–3.3	0.30–0.14
1.0 $[2, 0]^r$	0.83–0.68	5.0–4.1	0.72–0.80	2.4–2.7	0.23–0.13
0.5 $[2, 1]^r$	0.83–0.75	3.3–3.0	0.68–0.73	1.7–1.8	0.28–0.21
0.5 $[2, 1]^a$	0.78–0.56	3.1–2.3	0.70–0.76	1.7–1.9	0.25–0.20

^r radiative electrons ^a adiabatic electrons

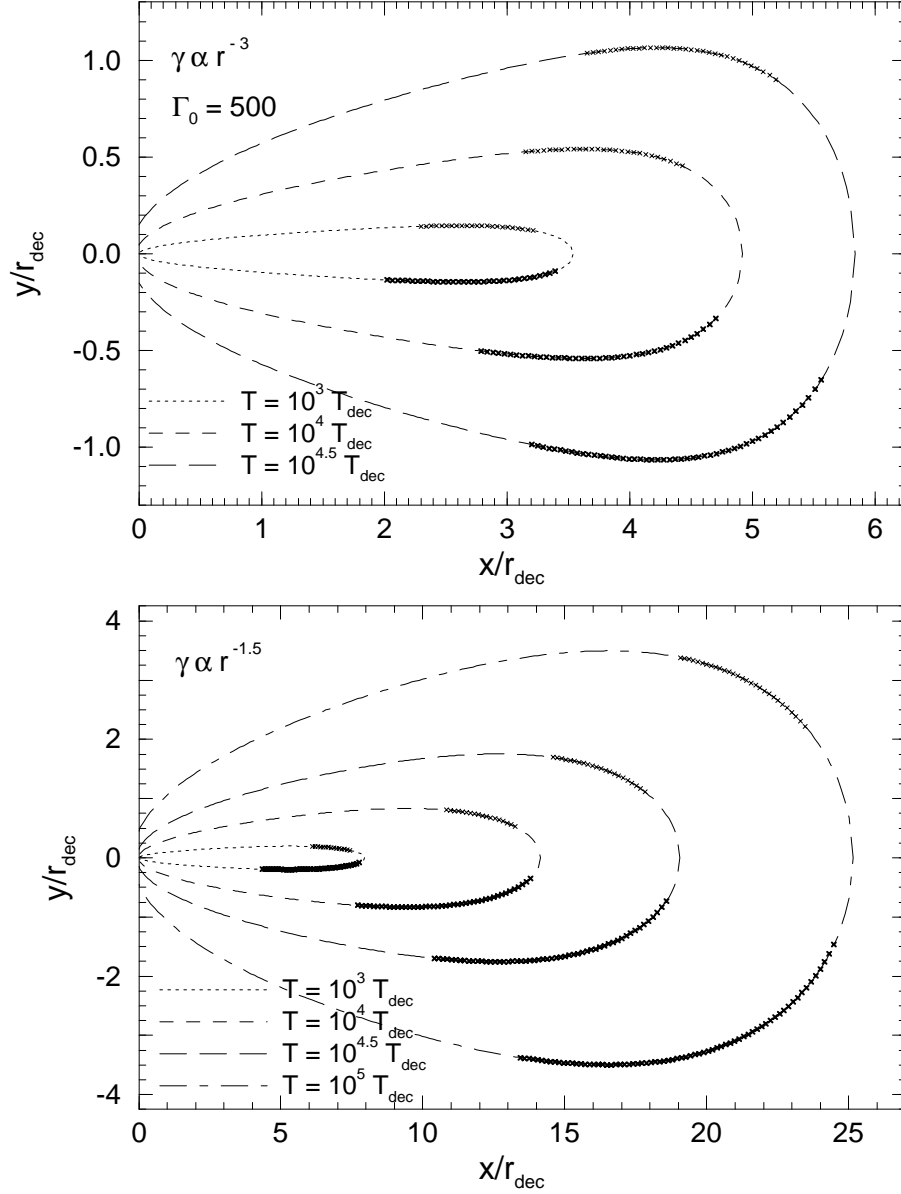


Fig. 1.— Surfaces of equal arrival times, for a homogeneous external medium and a radiative (top) or adiabatic remnant dynamics (bottom). Each curve is a transverse section through the 3-dimensional equal- T surface, highlighting the regions that radiate 50% (upper half of each curve) and 80% (lower half) of the bolometric flux. Projected on the plane perpendicular to the l.o.s. toward the center of explosion, these regions appear narrower than the projection of the entire radiating surface. The Cartesian coordinates are normalized to r_{dec} , which for the putative burst parameters in the text is $\sim 4 \times 10^{16}$ cm, corresponding at a redshift $z = 1$ ($H_0 = 75 \text{ km s}^{-1} \text{ Mpc}^{-1}$, $\Omega = 1$) to an angular scale $2.5 \mu\text{as}$.

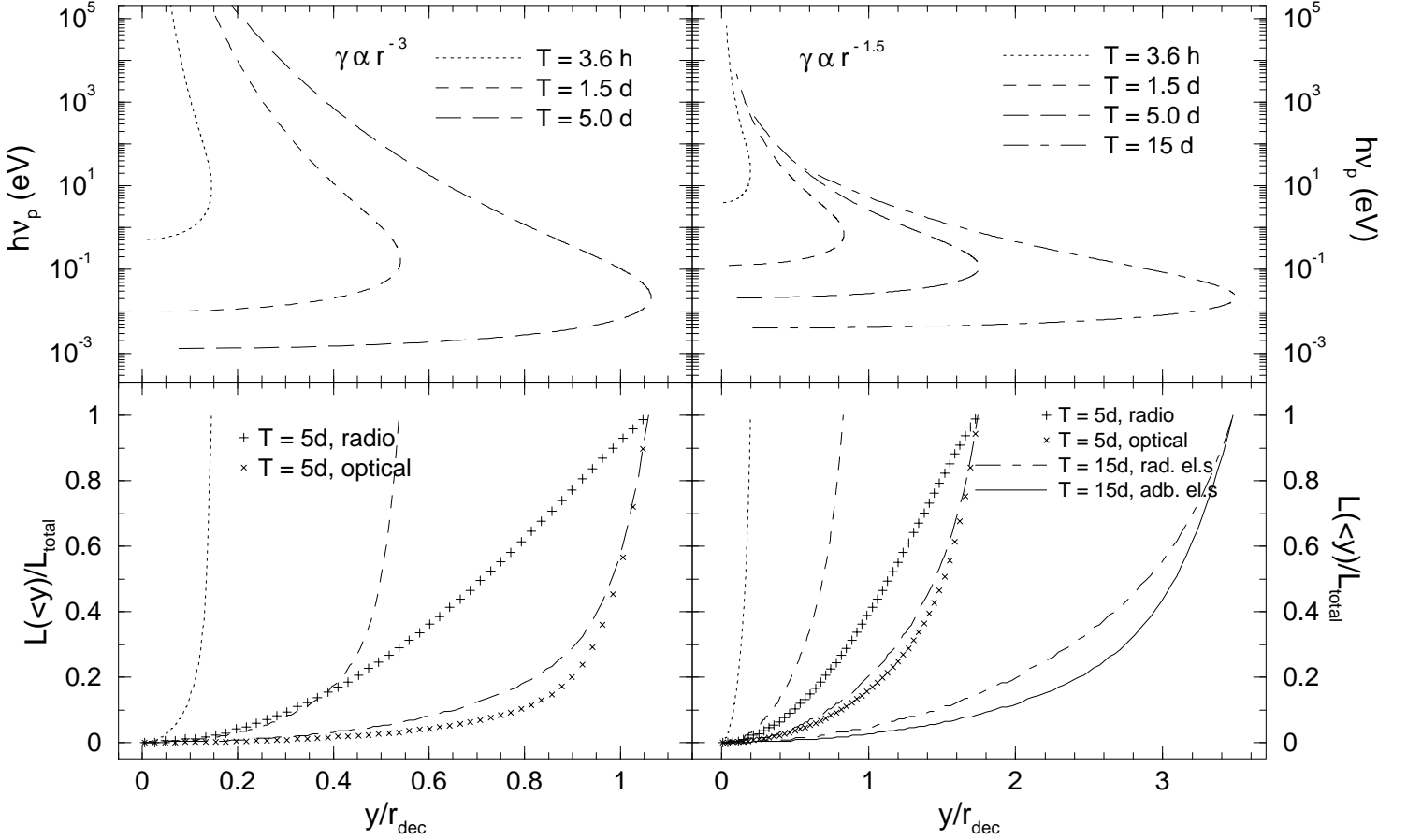


Fig. 2.— Distribution of peak of synchrotron spectrum on the equal arriving time surface (upper graphs) and bolometric luminosity on the same surface (lower graphs). Left panels are for a radiative remnant ($n = 3$), right panels for an adiabatic one ($n = 1.5$). The ring is shown by the steep rise in integrated bolometric luminosity in the lower graphs. Also shown in the lower graphs are the widths as observed in two fixed frequency bands (2 eV and 10 GHz). The lower right graph shows that if electrons are adiabatic (solid curve), then the bright zone shrinks to an even narrower ring.